Coupling Constant Corrections in a Holographic Model of Heavy Ion Collisions

Sašo Grozdanov[1] and Wilke van der Schee[2]
[1]Instituut-Lorentz for Theoretical Physics, Leiden University, Niels Bohrweg 2, Leiden 2333 CA, The Netherlands
[2]Center for Theoretical Physics, MIT, Cambridge, Massachusetts 02139, USA
(Received 2 November 2016; revised manuscript received 1 May 2017; published 6 July 2017)

We initiate a holographic study of coupling-dependent heavy ion collisions by analyzing, for the first time, the effects of leading-order, inverse coupling constant corrections. In the dual description, this amounts to colliding gravitational shock waves in a theory with curvature-squared terms. We find that, at intermediate coupling, nuclei experience less stopping and have more energy deposited near the light cone. When the decreased coupling results in an 80% larger shear viscosity, the time at which hydrodynamics becomes a good description of the plasma created from high energy collisions increases by 25%. The hydrodynamic phase of the evolution starts with a wider rapidity profile and smaller entropy.

DOI: 10.1103/PhysRevLett.119.011601

Introduction.—Relativistic collisions of heavy ions at RHIC and LHC result in the formation of a strongly interacting state of matter known as the quark-gluon plasma (QGP). While these experiments provide an invaluable window into properties of quantum chromodynamics (QCD), our theoretical understanding of QGP in QCD remains far from complete. In recent years, gauge-gravity duality (holography) has enabled theoretical studies of certain, usually supersymmetric, classes of large-N field theories, which are most readily performed at infinitely strong ('t Hooft) coupling λ. As a result of those advances, many properties of QGP previously conceived as impenetrably complex, such as its collective far-from-equilibrium behavior, can now be analyzed using numerical general relativity techniques. At infinite coupling, heavy ion collisions have been successfully modeled by (dual) collisions of gravitational shock waves in Einstein bulk theory with an extra dimension and a negative cosmological constant [1–5] (see [6–8] for reviews.).

We face several challenges in connecting holography with experimental studies of QGP, which typically occur at the intermediate coupling strength. Most formidable among them is establishing a bulk dual to nonsupersymmetric Yang-Mills theory with any (small) number of colors and fundamental matter. From the point of view of presently understood holography, even computing $1/N$ corrections around infinite N requires the inclusion of quantum gravity corrections (perturbative topological g_s corrections in string theory) (see, e.g., [9–11]). Including coupling constant corrections in a perturbative $(1/\lambda)$ series around infinite coupling is easier and requires one to find an α'-corrected higher-derivative supergravity action. To leading order, such coupling constant corrections have been computed for thermodynamics [12], hydrodynamics [13–18], thermalization, and higher-frequency spectrum at linear [19–21] and nonlinear levels [22]. Reference [21] further showed that simple leading-order higher derivative corrections to the bulk action reproduce a variety of coupling constant dependent phenomena, including the approach to kinetic theory regime and breakdown of hydrodynamics above a coupling-dependent critical momentum.

In this Letter, we describe the first dynamical (real-time) collision with coupling constant dependence. The dynamical nature allows us to see how the system evolves towards a hydrodynamic plasma, how the energy distributes itself, and to study the entropy production during the collision. What we will demonstrate is that, as the coupling constant is decreased, the nuclei experience less stopping with more energy deposited on the light cone and have a flatter distribution of energy in the plasma. The time until the effective hydrodynamic description becomes applicable (hydrodynamization time, t_{hyd}) is increased and less total entropy is produced.

Curvature-squared theories.—We will restrict our attention to the simplest, leading-order class of perturbative (in α') higher-derivative corrections and study curvature-squared theories. Such effective supergravity actions of massless modes, which are known to generically arise from string theory, can be found by either computing loop corrections to the world-sheet beta function [23,24] or by guessing the right action that could result in scattering amplitudes computed from string theory [25–27]. It is important to note that type IIB string theory compactified on S^5, dual to $\mathcal{N}=4$ SYM theory, is special from the point of view that all α' and α'^2 corrections vanish and the leading-order corrections are proportional to $\alpha'^3 R^4$ with $\alpha' \propto L^2/\lambda^{1/2}$. We adopt the view that it is plausible that in more realistic theories, such as in a putative dual to QCD, the leading order corrections would enter at order α', which is why we restrict to R^2 theories. Nevertheless, we wish to stress that a precise theory dual to these theories is unknown, even though the holographic framework allows us to compute field theory quantities, such as the expectation values of dual operators.

At leading order in α', the most general curvature-squared action can be written as the Einstein-Gauss-Bonnet theory [28]

$$S_{\rm GB} = \frac{1}{2\kappa_5^2}\int d^5x\sqrt{-g}\Big(R - 2\Lambda + \frac{\lambda_{\rm GB}}{2}L^2(R^2 - 4R_{\mu\nu}R^{\mu\nu} + R_{\mu\nu\rho\sigma}R^{\mu\nu\rho\sigma})\Big), \quad (1)$$

where the Gauss-Bonnet (GB) coupling $\lambda_{\rm GB} \propto \alpha'$, which we will treat perturbatively [29]. The negative cosmological constant $\Lambda = -6/L^2$ sets the anti–de Sitter scale, for which, to first order, we choose $L \equiv L_0 + \lambda_{\rm GB}L_1 = 1 + \lambda_{\rm GB}/2$ [33].

As discussed in [21,34], the Einstein-Gauss-Bonnet theory qualitatively reproduces the departure from infinitely coupled physics towards weaker coupling when $\lambda_{\rm GB} < 0$, including a larger shear viscosity $[\eta/s = (1/4\pi)(1 - 4\lambda_{\rm GB})]$ [14]. Despite the perturbative nature of our calculation in $\lambda_{\rm GB}$, for clarity, we will present results for $\lambda_{\rm GB} = -0.2$ and demonstrate convergence by computing the energy profiles up to $\mathcal{O}(\lambda_{\rm GB}^2)$. In $\mathcal{N} = 4$ theory, the value of the 't Hooft coupling that increases η/s by 80% is $\lambda \approx \mathcal{O}(10)$.

We work with a metric ansatz given in the characteristic formulation of [1,35] by

$$ds^2 = -Adt^2 + 2dt(dr + Fdz) + S^2(e^B d\mathbf{x}_\perp^2 + e^{-2B}dz^2), \quad (2)$$

where the functions A, B, F, and S all depend on the Eddington-Finkelstein time t, the (holographic) radial coordinate r, and the longitudinal coordinate z. Perturbatively (in $\lambda_{\rm GB}$), we write $A = A_0 + \lambda_{\rm GB}A_1$ and, similarly, for B, F, and S. After expanding the equations of motion derived from (1) to first order in $\lambda_{\rm GB}$, we have to solve two sets of differential equations. First, the standard nested set of ordinary differential equations (ODEs) for A_0, B_0, F_0, and S_0 [1], followed by an almost identical nested set of nonhomogeneous ODEs for A_1, B_1, F_1, and S_1. The nonhomogeneous terms depend on the numerical solution of the zeroth-order functions.

Once the solution is found, it is well known how to obtain the dual (conformal) holographic stress-energy tensor (see, e.g., [18,36]). We introduce a rescaled energy density

$$\mathcal{E} \equiv \frac{\kappa_5^2}{2L_0^3}T_{tt} = -\frac{3}{4}[a_{4,0} + \lambda_{\rm GB}(a_{4,1} - 2a_{4,0})], \quad (3)$$

where $a_{4,0}$ and $a_{4,1}$ are the normalizable modes of A_0 and A_1, respectively, with analogous formulas for the pressures. At $\lambda_{\rm GB} = 0$, the prefactor equals $2\pi^2/N_c^2$ for the dual $\mathcal{N} = 4$ SYM theory. For duals of the Einstein-Gauss-Bonnet theory, such a relation is unknown.

We are interested in studying the collision of planar sheets of energy, dual to the collision of gravitational shock waves. For our choice of L, the single shock wave metric in Fefferman-Graham coordinates [1,37] continues to be an exact solution of the equations of motion. These sheets of energy are characterized by a single nonzero component of the stress-energy tensor

$$T_{\pm\pm}(z_\pm) = \frac{\kappa_5^2}{2L_0^3}\frac{\mu^3}{\sqrt{2\pi w^2}}e^{-z_\pm^2/2w^2}, \quad (4)$$

with $z_\pm = t \pm z$ and w the width of the sheets. The sign in $z_\pm$ depends on the direction of motion of the shock. We can easily find a metric, such that the rescaled energy per transverse energy, μ^3, does not depend on $\lambda_{\rm GB}$ (this implies $a_{4,1} = 2a_{4,0}$, initially). These initial conditions can then be translated to Eddington-Finkelstein coordinates with the standard method explained in [38,39].

Heavy ion collisions at finite coupling.—We present results for narrow and wide shocks, with $\mu w = 0.1$ and $\mu w = 1.5$ [40]. Because of the Lorentz contraction at high energies, it is possible to think of narrow and wide shocks as of high- and low-energy heavy ion collisions, respectively. In Fig. 1, first, we present snapshots of the energy density

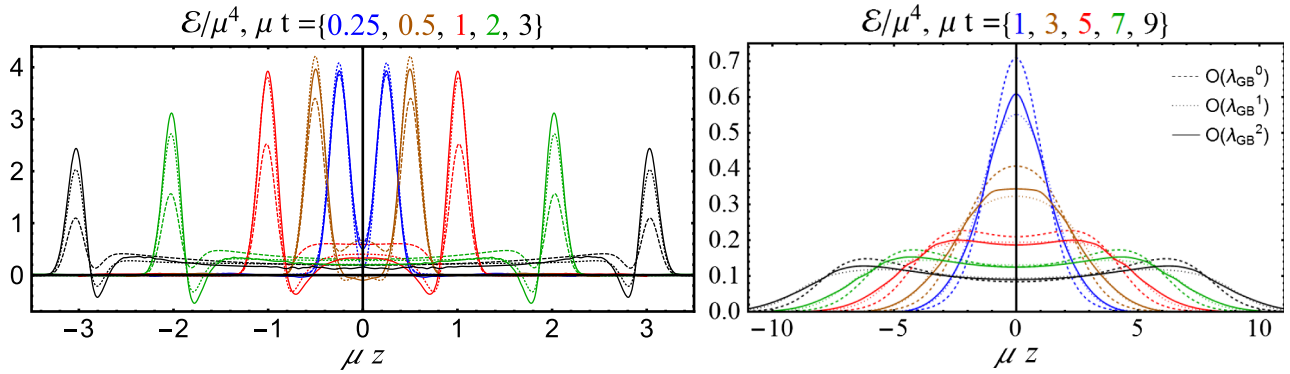

FIG. 1. Energy density along the longitudinal coordinate z at different times for narrow (left) and wide shock collisions (right). We present results for infinitely coupled (dashed lines), first-order corrected (dotted lines), and second-order corrected (solid lines) collisions at $\lambda_{\rm GB} = -0.2$. At intermediate coupling, we observe increased energy density near the light cones (peaks), which signals less stopping. In the plasma (between peaks), the energy density is flatter, which is caused by a smaller longitudinal pressure due to the larger viscosity.

profiles after collisions to $\mathcal{O}(\lambda_{\rm GB}^2)$ [41]. In [2,3], it was noticed that narrow shocks exhibit a transparent regime on the light cone as they pass through each other. At weaker coupling, we find that this effect of transparency is greatly enhanced. More precisely, for $\lambda_{\rm GB} = -0.2$, to leading-order in $\lambda_{\rm GB}$, the maximum energy density on the light cone is 88% higher at the end of our simulation than for $\lambda_{\rm GB} = 0$. The energy deposited in the plasma is, consequently, smaller, and we find its distribution to be flatter—a point to which we will return shortly. The difference between first and second order corrected results is small, but it is comforting to see that the second order result reduces the increase in energy on the light cone for the first order result around time $\mu t = 0.4$.

For wide shocks, the authors of Ref. [3] found a curious feature: not only did the energy come to a full stop and explode hydrodynamically, but due to the strong interactions, the energy piled up at midrapidity, leading to a maximum energy density of 2.71 times the maximum energy density of the incoming nuclei. Now, at weaker coupling, this effect subsides very rapidly; for $\lambda_{\rm GB} = -0.2$, the maximum $\mathcal{E}/\mu^4$ is only 2.17 times the initial maximum.

One of the hallmarks of infinitely strongly coupled collisions is its rapid relaxation towards a hydrodynamic regime (hydrodynamization). Given some temperature, this occurs within a time of $t_{\rm hyd} < 0.5/T$ at midrapidity—a result that is independent of the width of the shocks [3]. This comparison is usually done by comparing the full far-from-equilibrium pressure with the pressure that would follow from first-order hydrodynamics, given some temperature and fluid velocity. From our simulations, we extract the $\lambda_{\rm GB}$-dependent temperature, fluid velocity and viscosity. Combined, they allow us to compare the pressure (solid lines) with pressure computed from hydrodynamics (dashed lines), as shown in Fig. 2, for both $\lambda_{\rm GB} = 0$ (red) and $\lambda_{\rm GB} = -0.2$ (blue) (note that the longitudinal pressure follows from $\mathcal{E} = 2\mathcal{P}_T + \mathcal{P}_L$).

It is clear that, at intermediate coupling, it takes longer for hydrodynamics to become a good description of the evolution of the plasma. We quantify this by obtaining the time when hydrodynamics describes the transverse pressure within 10%, for small $\lambda_{\rm GB}$, which we find to be $\mu t_{\rm hyd} = \{1.48 - 1.1\lambda_{\rm GB}, 1.40 - 19\lambda_{\rm GB}\}$ for {narrow, wide} shocks. By further including the change in temperature, this leads to the hydrodynamization time in units of the temperature at the time of hydrodynamization

$$t_{\rm hyd} T_{\rm hyd} = \{0.41 - 0.52\lambda_{\rm GB}, 0.43 - 6.3\lambda_{\rm GB}\}, \quad (5)$$

again for {narrow, wide} shocks. For $\lambda_{\rm GB} = -0.2$, this results in 25% and 290% longer hydrodynamization times. The strong difference between wide and narrow shocks can be explained by realizing from Fig. 2 that wide shocks approach the hydrodynamic regime much slower due to the continuous inflow of matter. A coupling-dependent perturbation then leads to correspondingly larger

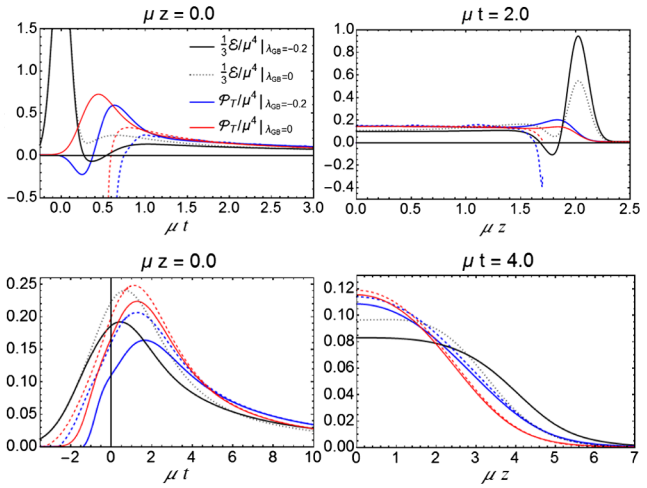

FIG. 2. Plots of infinitely coupled $\mathcal{E}/\mu^4$ (black, dotted line) and $\mathcal{P}_T/\mu^4$ (blue, solid line), and $\mathcal{E}/\mu^4$ (black, solid line) and $\mathcal{P}_T/\mu^4$ (red, solid line) at intermediate coupling, as well as hydrodynamic predictions for pressures (dotted line) as functions of time t and longitudinal coordinate z. Top plots represent narrow and bottom plots wide shocks. For narrow shocks, hydrodynamics breaks down near the light cone.

hydrodynamization times. Furthermore, the leading order $t_{\rm hyd} T_{\rm hyd} = 0.43$ for wide shocks is quite sensitive to our criterion for hydrodynamization and could be in the range of $t_{\rm hyd} T_{\rm hyd} = 0.0 - 2.0$ for similar criteria. This would greatly affect the 290% found at our 10% criterion. The result for narrow shocks has a very weak dependence on the width and the criterion used, making the increase of $t_{\rm hyd} T_{\rm hyd}$ by 25% more robust.

To set the initial conditions for the hydrodynamic evolution, it is crucial to obtain the rapidity distribution of the energy deposited in the plasma, which is shown in Fig. 3. We define rapidity y by $t = \tau \cosh y$ and $z = \tau \sinh y$, where τ is the proper time. At early times, the finite coupling corrections result in less energy deposited in the plasma, as well as in a wider rapidity profile (at its maximum, the rapidity profile is $\{11\%, 23\%\}$ wider for {narrow, wide} shocks). At late times, the increased viscosity at intermediate coupling plays an important role

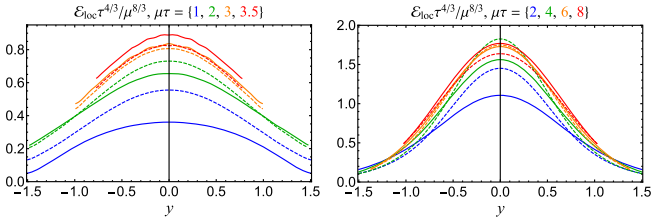

FIG. 3. Rapidity distributions (multiplied with $\tau^{4/3}$ to compensate for the expansion of the plasma) for narrow (left) and wide (right) shock collisions at $\lambda_{\rm GB} = -0.2$ (solid line) and $\lambda_{\rm GB} = 0$ (dashed line). The distributions start out wider and smaller, but become of comparable width and amplitude due to the 80% larger viscosity.

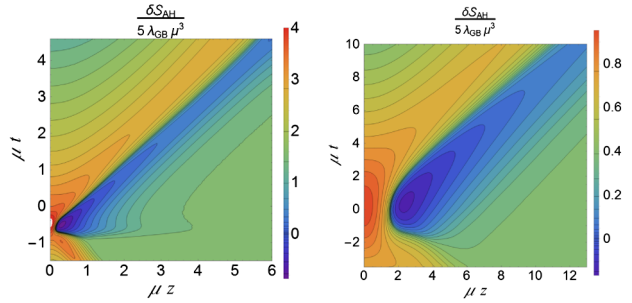

FIG. 4. Coupling constant correction to entropy density as measured by change in the area of the apparent horizon for narrow and wide shock waves. For negative $\lambda_{\rm GB}$, the entropy is enhanced at the light cone, while negative in the plasma. At even later times the entropy correction also becomes positive at midrapidity due to the larger viscous entropy production.

as it decreases the longitudinal pressure. The rapidity profile at $\lambda_{\rm GB} = 0$ grows faster in width and consequently has smaller energy density at midrapidity.

Another consequence of the increased viscosity can be seen in the entropy production. To demonstrate this, we show both the total entropy per transverse energy as a function of time (Fig. 5) and the difference in the entropy density $\delta s_{\rm AH}$ (Fig. 4) as measured by the apparent horizon and defined as

$$\delta\mathcal{S}_{\rm AH} \equiv \frac{\kappa_5^2}{2L_0^3}\delta s_{\rm AH} = 3\pi S_0^2(\lambda_{\rm GB}S_1 + \delta r_{\rm ah}\partial_r S_0). \quad (6)$$

All quantities are evaluated at the apparent horizon (AH) and $\delta r_{\rm ah}$ is the perturbation of its $\lambda_{\rm GB} = 0$ position that depends on t and z. It is clear from Fig. 4 that, for negative $\lambda_{\rm GB}$, there is more entropy near the light cone and less in the plasma—in agreement with Fig. 1. Overall, this leads to less total entropy, with 27% and 25% reduction for narrow and wide shocks at the start of our simulation. Because of larger viscous entropy production, this difference decreases in the hydrodynamic regime, and we find 15% and 12% reduction for narrow and wide shocks at the end of Fig. 5. The decrease can be partly explained by a reduced number of degrees of freedom, as our choice of L and $\lambda_{\rm GB}$ implies

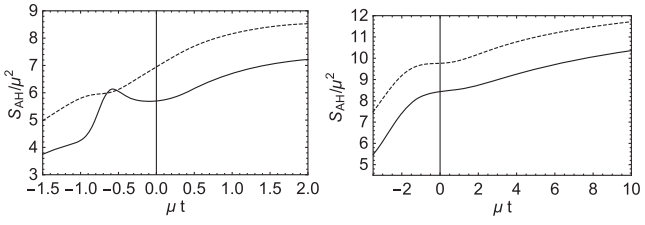

FIG. 5. Total entropy produced as measured by the apparent horizon area for narrow (left) and wide shocks (right) at $\lambda_{\rm GB} = -0.2$ (solid line) and $\lambda_{\rm GB} = 0$ (dashed line). The decrease in entropy around $\mu t = -0.5$ is expected to disappear in a simulation with a nonperturbative $\lambda_{\rm GB}$.

15% fewer degrees of freedom, as measured by T_{tt}/T^4. Last, we stress that Fig. 5 implies that the choice of $\lambda_{\rm GB} = -0.2$ is likely outside the regime of applicability of our first-order $\lambda_{\rm GB}$ expansion; we do not expect that the decrease of the entropy around $\mu t = -0.5$ would occur in a nonperturbative computation.

Discussion.—In this Letter, we presented the first computation of holographic heavy ion collisions at finite coupling, which amounted to solving the collision of gravitational shock waves in the Einstein-Gauss-Bonnet theory, perturbatively in $\lambda_{\rm GB}$. Interestingly, we found that the reduced coupling resulted in more energy on the light cone for narrow shocks, as well as less stopping for wider shocks, as measured by the reduced pileup of energy.

Our work sheds light on finite coupling corrections to strongly coupled phenomenology of heavy ion collisions, in particular, to its hydrodynamization times, its rapidity profile, and the entropy production (previously studied in [39,42–44]). In [42], it was found that the rapidity profile at strong coupling needed to be wider by about 50% to describe experimental data. Our results indeed indicate a wider initial rapidity profile, as is also suggested by the increased energy on the light cone for narrow shock collisions. Nevertheless, quantitatively, this increase only amounts to approximately 20%. Also, the increased viscosity leads to a reduced rapidity width and increased entropy production at later times, perhaps balancing each other at $\mu\tau = \{3, 6\}$ for {narrow, wide} shocks. However, in QCD, the quantitative size of these two effects can vary, especially as the shear viscosity of QCD in this regime is expected to decrease with decreasing temperature.

In this Letter, we considered only the simplest model for finite coupling corrections (perturbative curvature squared in pure gravity), studied it to next-to-leading-order in (inverse) perturbative coupling corrections and, thus, made the first step towards phenomenologically more accurate holographic models. Studying the theory nonperturbatively in $\lambda_{\rm GB}$ would be much more challenging, as the nested structure of the characteristic formulation of general relativity would be lost. In the future, it will also be important to compare our results to similar perturbative simulations in $\mathcal{N} = 4$ SYM theory. However, supported by the findings of Ref. [21], which analyzed the corrections to the linear spectrum from nonperturbative Gauss-Bonnet and perturbative α'^3 terms in type IIB supergravity (dual to $\mathcal{N} = 4$ SYM), we expect at least the qualitative behavior of shock wave collisions in top-down constructions to remain similar to the results of this Letter. It would also be interesting to study coupling corrections in nonconformal or charged theories (see [45,46]), which could model a varying viscosity as well as nontrivial baryonic charge densities.

Finally, a full description of the initial stages of heavy ion collisions will likely involve insights from both weakly and strongly coupled physics, and a complete description will then require an interpolation between physics found at

both weak and strong coupling, as, e.g., discussed in [47]. To make this interpolation, it will then be crucial to perform expansions both around $\lambda = 0$ as well as around $\lambda = \infty$. For dynamical far-from-equilibrium collisions, the latter expansion will follow the procedure that we initiated in this Letter.

We thank Jorge Casalderrey Solana, Andrei Starinets, and especially, Andrej Ficnar for helpful discussions. S. G. is supported by a VICI grant of the Netherlands Organization for Scientific Research (NWO), by the Netherlands Organization for Scientific Research/ Ministry of Science and Education (NWO/OCW) and by the Foundation for Research into Fundamental Matter (FOM). W. S. is supported by the U.S. Department of Energy under Grant Contract No. DE-SC0011090.

[1] P. M. Chesler and L. G. Yaffe, Phys. Rev. Lett. **106**, 021601 (2011).
[2] D. Grumiller and P. Romatschke, J. High Energy Phys. 08 (2008) 027.
[3] J. Casalderrey-Solana, M. P. Heller, D. Mateos, and W. van der Schee, Phys. Rev. Lett. **111**, 181601 (2013).
[4] J. Casalderrey-Solana, M. P. Heller, D. Mateos, and W. van der Schee, Phys. Rev. Lett. **112**, 221602 (2014).
[5] P. M. Chesler and L. G. Yaffe, J. High Energy Phys. 10 (2015) 070.
[6] J. Casalderrey-Solana, H. Liu, D. Mateos, K. Rajagopal, and U. A. Wiedemann, *Gauge/String Duality, Hot QCD and Heavy Ion Collisions* (Cambridge University Press, Cambridge, England, 2014).
[7] P. M. Chesler and W. van der Schee, Int. J. Mod. Phys. E **E24**, 1530011 (2015).
[8] M. P. Heller, Acta Phys. Pol. B **47**, 2581 (2016).
[9] F. Denef, S. A. Hartnoll, and S. Sachdev, Phys. Rev. D **80**, 126016 (2009).
[10] F. Denef, S. A. Hartnoll, and S. Sachdev, Classical Quantum Gravity **27**, 125001 (2010).
[11] P. Arnold, P. Szepietowski, and D. Vaman, J. High Energy Phys. 07 (2016) 032.
[12] S. S. Gubser, I. R. Klebanov, and A. A. Tseytlin, Nucl. Phys. **B534**, 202 (1998).
[13] Y. Kats and P. Petrov, J. High Energy Phys. 01 (2009) 044.
[14] M. Brigante, H. Liu, R. C. Myers, S. Shenker, and S. Yaida, Phys. Rev. D **77**, 126006 (2008).
[15] M. Brigante, H. Liu, R. C. Myers, S. Shenker, and S. Yaida, Phys. Rev. Lett. **100**, 191601 (2008).
[16] A. Buchel, R. C. Myers, M. F. Paulos, and A. Sinha, Phys. Lett. B **669**, 364 (2008).
[17] S. Grozdanov and A. O. Starinets, J. High Energy Phys. 03 (2015) 007.
[18] S. Grozdanov and A. O. Starinets, Teor. Mat. Fiz. **182**, 76 (2015); Theor. Math. Phys. **182**, 61 (2015).
[19] S. A. Stricker, Eur. Phys. J. C **74**, 2727 (2014).
[20] S. Waeber, A. Schaefer, A. Vuorinen, and L. G. Yaffe, J. High Energy Phys. 11 (2015) 087.
[21] S. Grozdanov, N. Kaplis, and A. O. Starinets, J. High Energy Phys. 07 (2016) 151.
[22] T. Andrade, J. Casalderrey-Solana, and A. Ficnar, J. High Energy Phys. 02 (2017) 016.
[23] C. G. Callan, Jr., C. Lovelace, C. R. Nappi, and S. A. Yost, Nucl. Phys. **B288**, 525 (1987).
[24] M. T. Grisaru and D. Zanon, Phys. Lett. B **177**, 347 (1986).
[25] D. J. Gross and J. H. Sloan, Nucl. Phys. **B291**, 41 (1987).
[26] D. J. Gross and E. Witten, Nucl. Phys. **B277**, 1 (1986).
[27] M. D. Freeman, C. N. Pope, M. F. Sohnius, and K. S. Stelle, Phys. Lett. B **178**, 199 (1986).
[28] Any perturbative R^2 theory can be conveniently transformed into the Einstein-Gauss-Bonnet theory (with second-order equations of motion). For details, see [14,17,21].
[29] Recently, [30] argued that (1) violates causality unless $|\lambda_{\rm GB}|/L^2 \ll 1$ (see, however, [31,32]). Since we work perturbatively in $\lambda_{\rm GB}$, such restrictions should not affect our findings.
[30] X. O. Camanho, J. D. Edelstein, J. Maldacena, and A. Zhiboedov, J. High Energy Phys. 02 (2016) 020.
[31] G. Papallo and H. S. Reall, J. High Energy Phys. 11 (2015) 109.
[32] T. Andrade, E. Caceres, and C. Keeler, arXiv:1610.06078.
[33] An advantage of this choice is that the nonnormalizable mode of the metric does not receive corrections.
[34] S. Grozdanov and A. O. Starinets, J. High Energy Phys. 03 (2017) 166.
[35] H. Bondi, Nature (London) **186**, 535 (1960).
[36] Y. Brihaye and E. Radu, Phys. Lett. B **661**, 167 (2008).
[37] R. A. Janik and R. B. Peschanski, Phys. Rev. D **73**, 045013 (2006).
[38] P. M. Chesler and L. G. Yaffe, J. High Energy Phys. 07 (2014) 086.
[39] W. van der Schee, Ph.D. thesis, Utrecht University, 2014, arXiv:1407.1849.
[40] For numerical stability, our simulations include a regulator energy density of less than 1% of the peak energy density. Further technical specifications, including the MATHEMATICA code used for the simulations, can be found on sites.google.com/site/wilkevanderschee/.
[41] The calculation to second order in $\lambda_{\rm GB}$ is entirely analogous to the first-order calculation described above. We expand $A = A_0 + \lambda_{\rm GB} A_1 + \lambda_{\rm GB}^2 A_2$ and set $L = 1 + \lambda_{\rm GB}/2 + 7\lambda_{\rm GB}^2/8$, which gives $\mathcal{E} = -\frac{3}{4}[a_{4,0} + \lambda_{\rm GB}(a_{4,1} - 2a_{4,0}) + \lambda_{\rm GB}^2(a_{4,2} - 2a_{4,1} - 2a_{4,0})]$. Thus, our initial conditions require setting $a_{4,2} = 2a_{4,1} + 2a_{4,0}$.
[42] W. van der Schee and B. Schenke, Phys. Rev. C **92**, 064907 (2015).
[43] S. S. Gubser, S. S. Pufu, and A. Yarom, Phys. Rev. D **78**, 066014 (2008).
[44] S. Lin and E. Shuryak, Phys. Rev. D **79**, 124015 (2009).
[45] M. Attems, J. Casalderrey-Solana, D. Mateos, D. Santos-Olivn, C. F. Sopuerta, M. Triana, and M. Zilho, J. High Energy Phys. 01 (2017) 026.
[46] J. Casalderrey-Solana, D. Mateos, W. van der Schee, and M. Triana, J. High Energy Phys. 09 (2016) 108.
[47] L. Keegan, A. Kurkela, P. Romatschke, W. van der Schee, and Y. Zhu, J. High Energy Phys. 04 (2016) 031.